Viscous heating of a laminar flow in the thermal entrance region of a rectangular channel with rounded corners and uniform wall temperature

Published Version:
Suzzi N., Lorenzini M. (2019). Viscous heating of a laminar flow in the thermal entrance region of a rectangular channel with rounded corners and uniform wall temperature. INTERNATIONAL JOURNAL OF THERMAL SCIENCES, 145, 1-10 [10.1016/j.ijthermalsci.2019.106032].

Availability:
This version is available at: https://hdl.handle.net/11585/725621 since: 2024-05-30

Published:
DOI: http://doi.org/10.1016/j.ijthermalsci.2019.106032

Viscous Heating of a Laminar Flow in the Thermal Entrance Region of a Rectangular Channel with Rounded Corners and Uniform Wall Temperature

Nicola Suzzi[a], Marco Lorenzini[b,*]

[a] *University of Udine - Derpartment of Electrical, Management and Mechanical Engineering Udine, Via delle Scienze 206, I-33100 Udine (UD), ITALY*
[b] *Alma Mater Studiorum - University of Bologna. DIN - Department of Industrial Engineering, Forlì Campus, Via Fontanelle 40, I-47121 Forlì (FC), ITALY*

Abstract

The numerical solution of Graetz-Brinkman problem is obtained for channels having rectangular cross section with rounded corners, under T boundary condition applied on the heated duct wall and adiabatic condition elsewhere, assuming an adiabatic preparation of the fluid at the inlet section. Several simulations are conducted and both Poiseuille and Nusselt numbers calculated, based on the computed velocity and temperature profiles. The numerical method is first verified with the resulting Nusselt and Poiseuille numbers with literature data, available for simplified configurations and fully developed flow, showing an excellent agreement. Comparison with numerical data is also conducted in case of fully developed flow and non-negligible viscous dissipation. A further validation is carried out comparing current computations with both experimental and numerical data in case of ther-

*Corresponding Author

Email addresses: `suzzi.nicola@spes.uniud.it` (Nicola Suzzi), `marco.lorenzini@unibo.it` (Marco Lorenzini)

mally developing flow inside a rectangular channel with negligible viscous heating (i.e. the well-known Graetz problem).
The effects of duct cross section geometry and Brinkman number are investigated and new correlations, useful for the design of microchannel heat sinks, are presented in order to predict the Poiseuille number and average Nusselt numbers.
Keywords: Microchannel, Graetz Problem, Viscous heating, Microconvection

---

1. Introduction

Microchannels are employed in a broad range of engineering applications. For example, heat sinks belonging to the so-called MFDs (micro-flow devices) are largely used for integrated cooling of small electronic components. New manufacturing processes, often originated in the semiconductor industry, allow fabrication of non-conventional silicon structures and channels of several cross-sections, [1], which, in turn, has given a new impulse to the investigation of single phase laminar forced convection through channels of various shapes, as testified by the literature. In fact, several research works investigate basic phenomena driving heat transfer and fluid flow in microchannels [2–14] and propose effective 1st- and 2nd-law based methods for optimization of channel geometry [15–20]. In [6] heat transfer through square and rectangular channels with rounded corners was numerically investigated: assuming fully developed flow, negligible axial conduction and applying H1 boundary conditions, the authors solved the governing Navier-Stokes equations over the 2D channel cross section domain and proposed new correlations for Poiseuille and Nusselt numbers as a function of joint radius. Temperature field in the restrictive case of rectangular channel section geometry and H2 boundary condition was analitically calculated in [2] and the resulting Nusselt number computed for different aspect ratios. A semi-analytical approach was used by Ray et al. [21] in order to solve the governing equations for a fully developed flow through square and equilateral triangular ducts with rounded corners under H1 and H2 boundary conditions. The influence of rarefaction on the Poiseuille number was numerically [7, 22], analytically [9] and experimentally [10] studied for rectangular, trapezoidal and elliptical ducts, with velocity-slip conditions being applied at the duct wall.

The effect of viscous dissipation in laminar forced convection through microchannels was studied by Morini [3] and a criterion to draw the limit of significance for viscous heating presented, while modified correlations for Nusselt number as a function of Brinkman number were presented in [5]: the author considered a fully developed flow through rectangular rounded channels with H1 boundary conditions and assumed non-negligible viscous heating effect. The combined effect of viscous dissipation and rarefied flow was studied in [8], where 2D Navier-Stokes equations for a fully developed flow through an elliptical channel are numerically solved by means of `COMSOL Multiphysics`®, applying velocity-slip condtition due to rarefaction effect and H2 thermal boundary condition; Nusselt number is thus traced as a function of both Knudsen and Brinkman numbers. A similar problem, i.e. fully developed flow through rectangular-shaped channels and non-negligible viscous heating, was numerically investigated by Barletta et al. [23], who solved the governing equations with H1 and T thermal boundary conditions using `FlexPDE`® and studied the effect of channel aspect ratio on the computed Nusselt number.

In the area of single phase laminar forced convection a number of scientific papers deals with thermally developing flow through channels, i.e. the so-called Graetz problem, which was solved analytically by Graetz and Nusselt more than a century ago in the simple case of circular ducts. An early work about thermally developing, laminar flow was presented by Michelsen et al. [24], who numerically investigated the extended Graetz problem for a fluid flowing in a circular tube with imposed wall temperature and uniform inlet temperature profile, when axial heat conduction cannot be neglected. The numerical results were presented in terms of local Nusselt number as a function of axial coordinate for different values of the non-dimensional Peclet number. A different extension of the Graetz problem was investigated in [25]: the authors assumed negligible axial heat conduction, but included the effect of viscous dissipation in the energy equation leading to the so-called Graetz-Brinkman problem, which may occur when micro-scales are involved. Thus, the momentum and energy equations were analytically solved for a circular tube, with both H2 and T boundary conditions being imposed at the channel wall. The Nusselt number was then expressed as a function of axial coordinate for different values of the Brinkman number, which compares viscous heating and heat conduction. The Graetz-Brinkman problem was also solved by Barletta et al. [23] in the case of parallel plates under T boundary conditions and adiabatic preparation of the fluid flow. Adopting a semi-analytical approach, the temperature field was decomposed into two contributions and the governing energy equation solved via separation of variables, which leads to an eigenvalue problem. Laminar forced convection inside non-circular tubes was numerically studied in [26–28], where the canonical Graetz problem (i.e. negligible axial conduction and viscous heating) was solved for different boundary conditions: Aparecido and Cotta [26] proposed a semi-analytic solution in case of rectangular ducts with T boundary condition imposed at the duct wall and uniform inlet temperature; Lee and Garimella [27] used `ANSYS Fluent`® in order to simulate channels having rectangular cross section under H1 boundary conditions applied at channel wall; Filali et al. [28] considered a non-linear viscoelastic fluid and numerically investigated circular, equilateral triangular and rectangular cross sections under H2 and T boundary conditions, looking for the influence of rheological parameters on heat transfer.

Different extensions of the Graetz problem can be found in literature: Aydin and Avci [29] and Barışık et al. [30] solved the so-called micro-Graetz-Brinkman problem, i.e. non-negligible axial conduction, viscous dissipation and rarefaction effects, in the restrictive case of a circular duct, imposing generalized Neumann condition at the duct wall. Such a boundary condition derives from the slip on both temperature and velocity fields occurring at duct wall due to rarefaction.

The aim of this work is the solution of the Graetz-Brinkman problem. Assuming laminar forced convection of a Newtonian fluid, neglecting axial conduction and rarefaction but accounting for viscous heating, the governing Navier-Stokes and energy equations are solved numerically. Rectangular ducts with rounded corners and three or four heated edges are considered, with a T thermal boundary condition applied along the heated perimeter.

Following [23], the method of separation of variables is applied in order to reduce the three-dimensional physical problem to a two-dimensional mathematical problem, resulting in a more efficient numerical solution in terms of computational costs. The local Nusselt number is computed as a function of axial coordinate and the effect of relevant non-dimensional parameters analysed, providing new correlations for Nusselt number prediction. It is important to point out that such a test case has never been investigated before. In fact, heat transfer performance of rectangular rounded ducts was studied for laminar, fully developed flow in [6], under the assumption of negligible viscous heating effect and H1 thermal boundary condition along heated perimeter, while the thermally developing flow problem with non-negligible viscous heating has been solved for simplified geometries only [23, 29, 30].

2. Mathematical model

Assuming that an incompressible, Newtonian fluid flows through the channel in steady, laminar, hydrodynamically developed regime, subject to no-slip at the wall and T thermal boundary condition (fixed temperature T_w at the heated portion of the channel wall) and neglecting axial conduction (x denoting the axial, or streamwise, coordinate), momentum and energy equations give,

$$\mu \left(\frac{\partial^2 u}{\partial y^2} + \frac{\partial^2 u}{\partial z^2} \right) - \frac{\partial p}{\partial x} = 0 \tag{1}$$

$$\rho\, c_p\, u \frac{\partial T}{\partial x} = k \left(\frac{\partial^2 T}{\partial y^2} + \frac{\partial^2 T}{\partial z^2} \right) + \mu\, \Phi \tag{2}$$

Φ being the viscous dissipation function:

$$\Phi = \left(\frac{\partial u}{\partial y} \right)^2 + \left(\frac{\partial u}{\partial z} \right)^2 \tag{3}$$

It is convenient to express the pressure gradient $\frac{\partial p}{\partial x}$, which is constant along the whole channel length L under the assumption of hydrodynamically developed flow, as a function of the friction factor and the bulk velocity:

$$\frac{\partial p}{\partial x} = \frac{\Delta p}{L} = \frac{1}{2}\, f\, \rho\, {u_b}^2 \frac{1}{D_h} \tag{4}$$

The following boundary conditions are applied at the channel wall:

$$u|_P = 0 \;:\; \text{no-slip condition at wall;} \tag{5}$$

$$T|_{P_h} = T_w \;:\; \text{fixed temperature along heated perimeter;} \tag{6}$$

$$\nabla T \cdot \hat{\boldsymbol{n}} = 0 \;:\; \text{adiabatic condition through } P - P_h. \tag{7}$$

The inlet temperature profile $T|_{x=0} = T_0(x, y)$ must be also imposed. Different inlet conditions may be investigated:

- uniform temperature profile, namely T_i, is usually imposed in the available literature dealing with Graetz problem;

- an adiabatic preparation of the fluid was introduced by Barletta et al. [23] for solving the Graetz-Brinkman problem in case of parallel plates, since it should lead to a more realistic configuration than a flat profile.

The same approach as [23] is here adopted. Thus, assuming an adiabatic preparation of the fluid, the energy equation at leading viscous effect,

$$k \left. \frac{\partial^2 T_0}{\partial y^2} + \frac{\partial^2 T_0}{\partial z^2} \right) + \mu\, \Phi = 0 \tag{8}$$

must be solved under adiabatic condition imposed along the channel section perimeter,

$$\nabla T_0 \cdot \hat{\boldsymbol{n}} = 0 \text{ through } P \tag{9}$$

in order to provide the inlet temperature profile $T_0(y,z)$.

By defining the following non-dimensional quantities,

$$\xi = \frac{x}{L};\ \eta = \frac{y}{D_h};\ \zeta = \frac{z}{D_h} \tag{10}$$

$$\tilde{u} = \frac{u}{u_b};\ \tilde{\Phi} = \left(\frac{D_h}{u_b}\right)^2 \Phi;\ \tilde{p} = \frac{\partial p}{\partial x}\frac{{D_h}^2}{\mu\, u_b};\ \Theta = \frac{T - T_w}{T_w - T_i} \tag{11}$$

and introducing the Brinkman, Graetz and Poiseuille numbers,

$$\mathrm{Br} = \frac{\mu\, u_b^2}{k\,(T_w - T_i)};\ \mathrm{Gz} = \mathrm{Re}\,\mathrm{Pr}\,\frac{D_h}{L};\ \mathrm{Po} = f\,\mathrm{Re} \tag{12}$$

Equations (1) and (2) can be rewritten in a non-dimensional form:

$$\frac{\partial^2 \tilde{u}}{\partial \eta^2} + \frac{\partial^2 \tilde{u}}{\partial \zeta^2} = -2\,\mathrm{Po} \tag{13}$$

$$\mathrm{Gz}\,\tilde{u}\,\frac{\partial \Theta}{\partial \xi} = \left.\frac{\partial^2 \Theta}{\partial \eta^2} + \frac{\partial^2 \Theta}{\partial \zeta^2}\right) + \mathrm{Br}\,\tilde{\Phi} \tag{14}$$

Boundary conditions can also be expressed in a non-dimensional fashon:

$$\tilde{u}\big|_{\partial\Omega} = 0\ :\ \text{no-slip condition at wall;} \tag{15}$$

$$\Theta\big|_{\partial\Omega_h} = 0\ :\ \text{fixed temperature along heated perimeter;} \tag{16}$$

$$\nabla\Theta \cdot \hat{\boldsymbol{n}} = 0\ :\ \text{adiabatic condition elsewhere, } \partial\Omega - \partial\Omega_h. \tag{17}$$

3. Temperature problem and Nusselt number

Following the approach of [23], the solution of Eqs. (13) and (14), subject to no-slip condition at wall and fixed wall temperature, is sought in the form,

$$\Theta = \Theta_v + \Theta_c \tag{18}$$

where:

- Θ_v is the $\xi-$independent solution of the partial differential equation describing the effects of viscous heating on the temperature field

$$\frac{\partial^2 \Theta_v}{\partial \eta^2} + \frac{\partial^2 \Theta_v}{\partial \zeta^2} + \mathrm{Br}\, \tilde{\Phi} = 0 \tag{19}$$

$$\tilde{\Phi} = \left(\frac{\partial \tilde{u}}{\partial \eta}\right)^2 + \left(\frac{\partial \tilde{u}}{\partial \zeta}\right)^2 \tag{20}$$

with uniform wall temperature imposed along the heated perimeter and adiabatic conditions everywhere else;

- Θ_c is the solution of the energy equation with negligible viscous heating effect,

$$\mathrm{Gz}\, \tilde{u}\, \frac{\partial \Theta_c}{\partial \xi} = \frac{\partial^2 \Theta_c}{\partial \eta^2} + \frac{\partial^2 \Theta_c}{\partial \zeta^2} \tag{21}$$

with uniform wall temperature imposed along the heated perimeter and adiabatic conditions elsewhere too over the channel wall. According to adiabatic preparation of the fluid, the additional inlet temperature profile, $\Theta|_{\xi=0} = \Theta_0(\eta, \zeta)$ is obtained via the solution of:

$$\frac{\partial^2 \Theta_0}{\partial \eta^2} + \frac{\partial^2 \Theta_0}{\partial \zeta^2} + \tilde{\Phi} = 0 \tag{22}$$

$$\nabla \Theta_0 \cdot \hat{\boldsymbol{n}} = 0 \,\mathrm{on}\, \partial\Omega \tag{23}$$

Following [23], Θ_c can be computed via separation of variables,

$$\Theta_c = \sum_{n=0}^{+\infty} C_n\, \alpha_n(\xi)\, \psi_n(\eta, \zeta) \tag{24}$$

where C_n are constants depending on the prescribed temperature distribution imposed at the inlet section and α_n is equal to:

$$\alpha_n = \exp\left(-\frac{\lambda_n}{\mathrm{Gz}}\, \xi\right) \tag{25}$$

Thus, Eq. (21) can be reduced to the following eigenvalue problem,

$$\frac{\partial^2 \psi_n}{\partial \eta^2} + \frac{\partial^2 \psi_n}{\partial \zeta^2} + \lambda_n \, \tilde{u} \, \psi_n = 0 \tag{26}$$

with a T thermal boundary condition imposed along the heated perimeter:

$$\begin{aligned} {}_n &= 0 \text{ on } \partial\Omega_h \\ \nabla \psi_n \cdot \hat{\boldsymbol{n}} &= 0 \text{ on } \partial\Omega - \partial\Omega_h \end{aligned} \tag{27}$$

Equations (13), (19) and (26) must be solved and the coefficients C_n and eigenvalues λ_n computed, yielding the velocity field $\tilde{u}(\eta, \zeta)$ and the temperature field $\Theta(\xi, \eta, \zeta)$.

Thus, the average Nusselt number can be computed over the channel length as,

$$\mathrm{Nu} = \frac{q_w \, D_h}{k \, (T_w - T_b)} \tag{28}$$

where q_w represents the average heat flux through wall, defined through integration of the Fourier law along channel section perimeter,

$$q_w = -\frac{k \; (T_w - T_i)}{D_h} \, \frac{1}{\partial\Omega_h} \int_{\partial\Omega} \nabla\Theta \cdot \hat{\boldsymbol{n}} \, d\Gamma \tag{29}$$

with $d\Gamma = \frac{dl}{D_h}$ the non-dimensional tangential direction to the cross-section perimeter.

Following [23], the non-dimensional temperature can be decomposed according to Eq. (18) and the average Nusselt number reduced to,

$$\mathrm{Nu} = \frac{\mathrm{Nu}_v \, \Theta_{b,v} + \mathrm{Nu}_c \, \Theta_{b,c}}{\Theta_{b,v} + \Theta_{b,c}} \tag{30}$$

where:

- Nu_v, which is the Nusselt number related to viscous heating, can be calculated as,

$$\mathrm{Nu}_v = \frac{\frac{1}{\partial\Omega_h}\ \int_\Omega \mathrm{Br}\,\tilde{\Phi}\,d\Omega}{\Theta_{b,v}} \tag{31}$$

  $\Omega = A_c/{D_h}^2$ being the non-dimensional channel section area, $\partial\Omega_h$ the non-dimensional heated perimeter and $\Theta_{b,v}$ the bulk temperature:

$$\Theta_{b,v} = \frac{\int_\Omega \tilde{u}\,\Theta_v\,d\Omega}{\int_\Omega \tilde{u}\,d\Omega} \tag{32}$$

- Nu_c, which is the Nusselt number resulting from solution of the eigenvalue problem described by Eq. (26), is given by:

$$\mathrm{Nu}_c = \frac{\sum_{n=0}^{+\infty}\left(\frac{\lambda_n}{4}\frac{P_h}{P}\right)\quad_{b,n}\ \exp\left(-\frac{\lambda_n}{\mathrm{Gz}}\xi\right)}{\Theta_{b,c}} \tag{33}$$

  λ_n corresponds to the n-th eigenvalue, with $\quad_n$ the n-th eigenfunction. Thus, we have:

$$_{b,n} = \frac{C_n\ \int_\Omega \tilde{u}\,\psi_n\,d\Omega}{\int_\Omega \tilde{u}\,d\Omega} \tag{34}$$

  $\Theta_{b,c}$ is the bulk temperature, which depends on channel axial coordinate ξ according to:

$$\Theta_{b,c} = \sum_{n=0}^{+\infty}\quad_{b,n}\ \exp\quad -\frac{\lambda_n}{\mathrm{Gz}}\xi\Bigg) \tag{35}$$

Computing Nu_v through Eq. (31), i.e. using the total thermal power generated by viscous dissipation, which is an integral quantity, and the bulk temperature, rather than integrating the local heat flux through the heated perimeter, ensures a more accurate estimation when post-processing numerical data. For the same reason, it is convinient to compute Nu_c through Eq. (33), which refers to integral quantities too. It is also worth pointing out that the mean Nusselt number at negligible viscous heating for a fully developed flow (i.e. at a distance $x \to \infty$ from the inlet section) can be calculated, according to Eq. (33), as a function of the first eigenvalue λ_1:

$$\mathrm{Nu}_c \xrightarrow{x\to\infty} \left. \frac{\lambda_1}{4} \frac{P_h}{P} \right) \tag{36}$$

4. Numerical method

Governing equations, Eqs. (13), (19) and (26) can not be analitically solved but in few cases: circular and rectangular channel cross-sections, with Green's functions generally used in the latter case. Since we want to investigate the effect of smoothing the corners of a partially heated rectangular shaped channel (leading to a more complex geometry, as shown in figure 1), a numerical approach must be adopted in order to assess both the velocity and temperature fields. Thus, Eqs. (13), (19) and (26) are numerically solved using the available FEM solvers and mesh generator included in the pdetool package of `MATLAB`® . An initial triangular mesh discretizing the 2D channel section is first generated.

Solution of momentum equation, Eq. (13), is iterated until the guessed Poiseuille number is such that

$$\mathrm{Po}\,:\,\tilde{u}_b = \frac{1}{\Omega}\int_\Omega \tilde{u}\,d\Omega \simeq \frac{1}{\Omega}\sum_{i=1}^{n_e}\tilde{u}_i\,d\Omega_i = 1 \tag{37}$$

with $i \in [1, n_e]$ denoting the $i-$th mesh element. The energy equation for viscous heating, Eq. (19), with imposed wall temperature is numerically solved on the same mesh grid as that for Eq. (13) since the velocity field is required to compute viscous dissipation function. The `MATLAB`® function `@adaptmesh` is used in order to solve Eqs. (13) and (19) with an adaptive triangular mesh method, the initial mesh being progressively refined in order to get a more accurate solution.

The eigenvalue problem, given by Eqs. (26) and (27), is solved using `@pdeeig`, which returns both the eigenvalues λ_n and the eigenfunctions ψ_n, on the same mesh as that employed for momentum equation, Eq. (13), with the velocity field being required to compute the non-linear coefficient in Eq. (26).

Once the eigenfunctions ψ_n, the corresponding eigenvalues λ_n and the temperature field for viscous heating Θ_v are computed, the coefficients C_n can be determined so as to satisfy the imposed inlet temperature distribution (the function `@lsqnonlin`, belonging to the `MATLAB`® optimization toolbox, is used for such a purpose), allowing to calculate the non-dimensional temperature field Θ inside the channel as:

$$\Theta = \Theta_v(\eta,\zeta) + \sum_n C_n\,\psi_n(\eta,\zeta)\,\exp\left(-\frac{\lambda_n}{\mathrm{Gz}}\xi\right) \tag{38}$$

Since decomposing temperature field into two contributions, Eq. (18), and applying separation of variables, Eq. (24), leads to two PDEs to be solved on a 2D computational domain together with momentum PDE, the proposed numerical procedure is much more efficient than a fully 3D approach in terms of computational costs, allowing for investigation of a wide range of configurations.

5. Investigated setup

Two different sets of geometry describing real configurations are investigated:

- 3T: channel section identified by a rectangular shape with 2 rounded corners, Fig. 1(a);

- 4T: channel section identified by a rectangular shape with 4 rounded corners, Fig. 1(b).

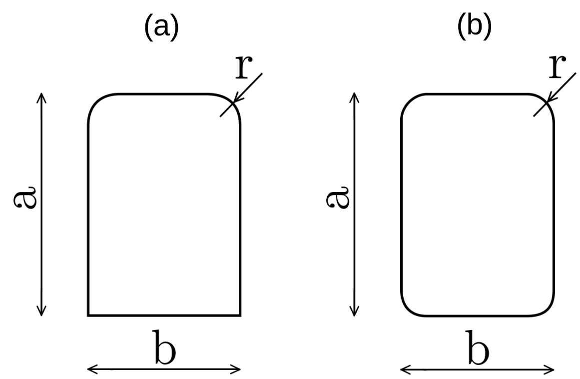

Figure 1: Investigated channel geometries: rectangular shape with 2 rounded corners (a); rectangular shape with 4 rounded corners (b).

Geometry characteristics are identified in terms of aspect ratio β and non-dimensional radius of curvature γ,

$$\beta = \frac{b}{a};\ \gamma = 2\,\frac{r}{b} \tag{39}$$

with b the shorter edge of the reference rectangular cross-section.
The no-slip condition at channel wall is used in all instances,

$$\tilde{u}|_{\partial\Omega} = 0 \tag{40}$$

whilst two different sets of boundary conditions concerning temperature field are investigted:

- referring to Fig. 1(a), the T boundary condition is imposed along the heated cross section perimeter, whilst the adiabatic condition is applied on the short edge of the channel cross section having sharp corners,

$$\begin{aligned} \Theta|_{\partial\Omega_h} &= 0 \\ \nabla\Theta \cdot \hat{\boldsymbol{n}} &= 0 \text{ on } \partial\Omega - \partial\Omega_h \end{aligned} \tag{41}$$

$\hat{\boldsymbol{n}}$ being the normal inward direction to the duct cross section.

- referring to Fig. 1(b), wall temperature T_w is imposed along whole channel cross section perimeter, leading to T boundary condition:

$$\Theta|_{\partial\Omega} = 0 \tag{42}$$

Adiabatic preparation of the fluid is imposed and the inlet temperature profile computed through Eqs. (22) and (23), with the non-dimensional viscous dissipation function $\tilde{\Phi}$ in Eq. (22) estimated from the known developed velocity profile. Since Eqs. (22) and (23) admit infinite solutions, the following condition was imposed in order to compute inlet profile Θ_0,

$$\frac{1}{\Omega} \int_\Omega \tilde{u}\, \Theta_0 \, d\Omega = -1 \tag{43}$$

which means that bulk temperature of incoming fluid corresponds to the reference inlet temperature T_i.

6. Model verification and validation

6.1. Fully developed flow

The numerical procedure was first verified with some experimental results from the literature, which cover simple geometry configurations. Comparison with numerical results is also conducted when viscous heating and complex coss-sectional geometry are involved. The Poiseuille and Nusselt numbers for a fully developed flow through a rectangular cross-section with sharp corners, i.e. $\gamma = 0$, are available for different aspect ratios β, when viscous heating is negligible (i.e. $\mathrm{Br} = 0$) and wall temperature imposed along 3 or 4 edges [31, 32]. Barletta et al. [33] numerically investigated the case of hydrodynamically and thermally developed flow through a channel with dominant viscous heating. The channel geometry was rectangular with four rounded corners, $\beta \in [0.05, 1]$ and $\gamma = 1$, and uniform wall temperature along the whole perimeter: under the above mentioned assumption, Nusselt number does not change along the axial coordinate and depends on the geometry of the channel's cross-section only, regardless of the the magnitude of the Brinkman number.

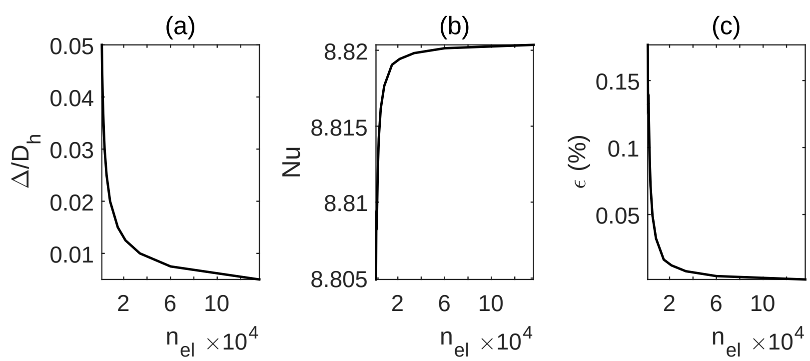

Figure 2: Mesh accuracy parameter versus number of triangular elements (a), developed Nusselt number (b) and estimation error (c) as a function of elements number. Test case 3T, $\beta = 3/5$, $\gamma = 2/3$.

After setting the accuracy of `MATLAB`® mesh generator in order to ensure grid independence (namely reached when computed Poiseuille and Nusselt numbers are no more affected by mesh progressive refinement), numerical results are compared to the results reported in [33] and [31] in terms of both Poiseuille and Nusselt numbers. A grid dependence analysis was conducted: the accuracy parameter of MATLAB® gridder @generateMesh (i.e. the maximum distance between two neightbour nodes, namely Δ/D_h) was progressively increased and both average Nusselt number at leading viscous heating and estimation error were traced as a function of mesh elements, as shown in Fig. 2, finding a discrepancy of about 0.0076% on the estimated Nu when $\Delta/D_h = 10^{-2}$. Using adaptive mesh option, i.e. @adaptmesh function, always ensures higher accuracy than @generateMesh for a given number of mesh elements.

β	Po		Nu_v	
0.05	22.87[33]	22.87	16.21[33]	16.21
0.1	21.85[33]	21.86	15.07[33]	15.06
0.2	20.13[33]	20.13	13.18[33]	13.18
0.3	18.78[33]	18.78	11.80[33]	11.80
0.4	17.76[33]	17.76	10.86[33]	10.86
0.5	17.03[33]	17.03	10.26[33]	10.26
0.6	16.54[33]	16.54	9.906[33]	9.906
0.7	16.24[33]	16.24	9.714[33]	9.714
0.8	16.08[33]	16.08	9.628[33]	9.627
0.9	16.01[33]	16.01	9.602[33]	9.601
1	16.00[33]	16.00	9.600[33]	9.600

Table 1: Computed vs literature Poiseuille and Nusselt numbers in case of: dominant viscous heating; wall temperature imposed; 4T, $\gamma = 1$.

Tables 1 and 2 show a perfect agreement with both the numerical results

β	Po		Nu_c			
0.1	21.17[31]	21.17	–	5.908	6.095[31]	6.189
0.2	19.07[31]	19.07	–	4.829	5.195[31]	5.256
0.3	17.51[31]	17.51	–	4.130	4.579[31]	4.626
1/3	17.09[31]	17.09	3.956[31]	3.958	–	4.464
0.4	16.37[31]	16.37	–	3.681	4.154[31]	4.191
0.5	15.55[31]	15.55	3.391[31]	3.392	3.842[31]	3.874
0.7	14.61[31]	14.61	–	3.091	3.408[31]	3.432
1/1.4	14.56[31]	14.57	3.077[31]	3.078	–	3.407
1	14.23[31]	14.23	2.976[31]	2.978	3.018[31]	3.025

Table 2: Computed vs literature Poiseuille and Nusselt numbers in case of: negligible viscous heating; 3 and 4 heated edges; $\gamma = 0$.

of [33] and the analytical values of [31] in terms of Poiseuille number for all the geometries investigated. Computations of the Nusselt number at dominant viscous heating, Nu_v, also reveals sufficient accuracy compared to the numerical results of [33], as shown in Table 1, as well as the Nusselt number at negligible viscous heating, Nu_c, whose estimation is verified with the literature, analytical values of [31] in case of rectangular cross section and 4 heated edges, as shown in Table 2; Nu_c for a circular shape was also verified to converge asymptotically to the well-known value of 3.66 for increasing mesh refinement. More uncertainty on the computed Nusselt number Nu_c was found when 3 edges are heated (with temperature imposed along the heated perimeter and adiabatic condition imposed elsewhere), the discrepancy with values of [31] ranging between $0.2-1.5\,\%$ as clearly shown in Table 2. However, such a discrepancy can be found even comparing literature results of [31] with those of [32], when T boundary conditions are applied over the whole cross-sectional perimeter.

6.2. Thermally developing flow

The mathematical model is also validated with experimental evidences in case of thermally developing flow and fixed wall temperature boundary condition along the whole section perimeter. Exept for the limiting case of circular duct, literature data are only provided in case of rectangular cross section channels and negligible viscous heating. Thus, Eqs. (21) and (13) are numerically solved. The case of rectangular cross section characterized by aspect ratio $\beta = 1/2$ is chosen. Since viscous heating is neglected, $\mathrm{Br} = 0$, an uniform inlet temperature profile is imposed. The first 64 eigenfunctions, deriving from solution of eigenvalue problem, Eq. (26), are used for the imposition of inlet condition.

In figure 3, the resulting logarithmic Nusselt number Nu_l is plotted as a function of axial length and compared with experimental points printout in [34]. $\mathrm{Nu}_l = h_l\, D_h/k$ can be easily computed by writing macroscopic energy balance,

$$\dot{Q}_w = \dot{m}\, c_p\, (T_i - T_b) = P\, x\, h_l\, \Delta T_l \tag{44}$$

ΔT_l being the logarithmic mean temperature:

$$\Delta T_l = \frac{\Delta T_i - \Delta T_b}{\log\left(\frac{\Delta T_i}{\Delta T_b}\right)} \tag{45}$$

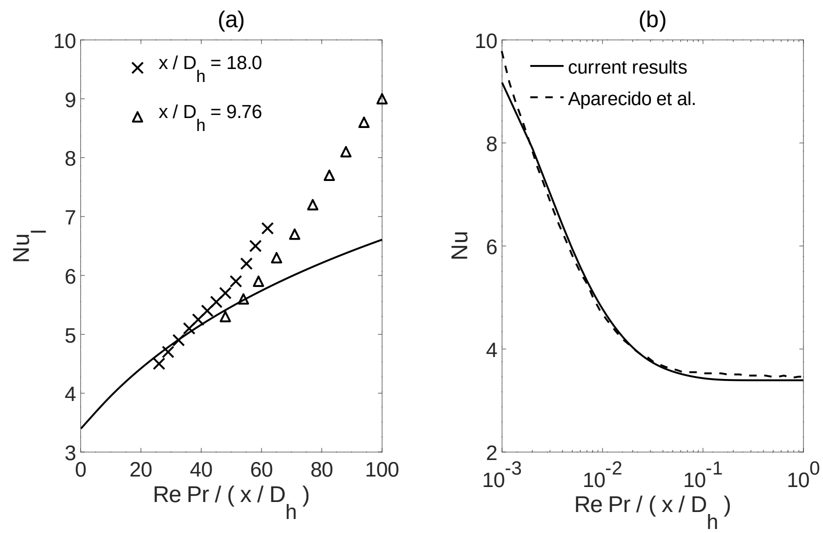

Figure 3: Computed logarithmic mean Nusselt number (continuous line) versus experimental data (markers) of [34] (a). Computed local Nusselt number versus numerical results of [26] along channel non-dimensional axial direction (b). T boundary condition, $\beta = 1/2$, $\gamma = 0$, $\mathrm{Br} = 0$.

Expressing h_l through the energy balance and using non-dimensional quantities, the logarithmic mean Nusselt number becomes:

$$\mathrm{Nu}_l = -\frac{1}{4}\,\mathrm{Re}\,\mathrm{Pr}\,\frac{D_h}{x}\;\log\Theta_b \tag{46}$$

It can be noticed that the logarithmic Nusselt number, as well as the bulk temperature along channel θ_b, univocally depends on the non-dimensional axial coordinate $\tilde{x}$:

$$\tilde{x} = \frac{x}{D_h}\,\mathrm{Re}\,\mathrm{Pr} \tag{47}$$

However, different values of Nu_l were experimentally obtained in [34] for a prescribed value of $\tilde{x}$, since experimental points are referred to different liquid flow rates $\dot{m}$. Such a discrepancy, which is not predicted by the mathematical model, is due to the increasing Reynolds number, which is proportional to $\dot{m}$ according to $\mathrm{Re} = \dot{m}\, D_h/(\mu\, A_c)$, with higher values of the investigated Re approaching the laminar-turbulent transition value. In fact, the discrepancy between numerical and experimental results is lower than 10% for $\mathrm{Re} < 10^3$. Figure 4 compares the resulting local Nusselt number, computed through Eq. (33), with the numerical results of [26], which authors numerically solved Eqs. (21) and (13), under the same boundary condition as here, using the generalized integral transform technique in order to reduce the costs of computations. A good agreement can be observed in both the entry region and the fully developed value of the Nusselt number.

7. Results and discussion

Equations (19) and (21) are numerically solved together with momentum equation, Eq. (13), and the resulting solutions Θ_c and Θ_v combined in order to define the temperature field Θ.

Numerical results shown in figures 4, 5 and 6 all refer to the conditions listed below, which have not been investigated so far in the open literature:

- Case 3T: rectangular section with 2 rounded corners and 3 edges heated, see Fig. 1(a);
- Inlet condition: adiabatic preparation, see Eqs. (22) and (23);
- Channel aspect ratio: $\beta = 3/5$;
- Non-dimensional joint radius: $\gamma = 2/3$;
- Graetz number: $\mathrm{Gz} = 3.5$;

- Brinkman number: Br $= 0.1$.

Inlet temperature profile (i.e. at $x = 0$) is shown in Fig. 4(a), while fully developed velocity and temperature profiles (corresponding to infinite channel length, $x \to \infty$) are shown in Figs. 4(b) and 4(c) respectively. Note that the imposed inlet temperature field, which derives from imposition of adiabatic preparation, is not uniform and requires additional numerical investigation. In fact $\Theta_0(\eta, \zeta)$ is not known a priori and Eq. (19) must be solved under adiabatic condition applied at channel section perimeter. Fig. 4(a) actually provides the numerically computed profile Θ_0, which must be fitted using the eigenfunctions ψ_n from the solution of Eqs. (26) and (27) together with the contribution of Θ_v, in order to impose the inlet condition when solving energy equation inside the channel,

$$C_n \,:\, \min\left\{\sum_i {\epsilon_i}^2\right\},\, \epsilon_i = \Theta_{0,i} - \sum_n C_n\, \psi_{n,i} \tag{48}$$

with i denoting the mesh element.

Actually, the first 50 eigenfunctions $\ _n$ deriving from Eq. (26) were used. Following the procedure of [23], where the number of eigenfunctions were set to 20 only, it was first verified that using 60 eigenfunctions instead of 50 does not lead to significant improvement (namely $< 0.01\%$) in terms of computed Nusselt number at $x/D_h > 0.001\,\mathrm{Pe}$, meaning that sufficient accuracy is reached. We decided to evaluate the accuracy on the estimated Nu, since it is the relevant quantity we want to extrapolate from computation so far. However, the truncation error,

$$\epsilon = \frac{|\Theta_0 - (\Theta_v + \sum_n C_n \quad_n)|}{|\Theta_0|} \tag{49}$$

was also compuetd for different numbers of ψ_n (needed to fit the imposed Θ_0), in order to verify the proper imposition of the desired inlet temperature profile, finding that $\epsilon_{50} = 0.1341$ (with the cross-section geometry discretized using more than 15000 triangular elements) and $\frac{\Delta\epsilon}{\Delta n} = \frac{\epsilon_{50}-\epsilon_{60}}{10} \simeq 1.1 \times 10^{-3}$ (thus, the truncation error would slowly decrease for increasing number of eigenfunctions).

Looking at the fully developed temperature profile, figure 4(c), it is important to point out that the fluid becomes warmer than the duct at $x \to \infty$, owing to the effect of viscous heating. In fact, the fluid is progressively heated due to the heat exchange through duct walls in the thermal entrance region, whilst heat generation due to viscous dissipation (acting as source term in the energy equation) is the dominant effect when the bulk temperature approaches the imposed wall temperature T_w. Computed Poiseuille number, which is uniform along channel axial direction, assumes the value of Po $= 15.691$. Local Nusselt number along heated perimeter of the duct cross section is numerically computed from the fully-developed temperature profile. Comparing its behaviour, Fig. 5(b), to the corresponding channel section geometry, Fig. 5(a), it can be noticed that the maximum value of Nu is symmetrically reached along the two longer edges, where the temperature gradient is at its highest.

Non-dimensional temperature as a function of axial coordinate is also computed along the thermal entrance region. Figure 6(a) shows the temperature profile over the vertical mid-plane of the channel: as mentioned above, heat is transferred from the duct wall to the fluid flow until viscous heating becomes the dominant effect driving heat transfer. The mean Nusselt number along the channel length is numerically computed through Eqs. (30), (31) and (33) and is plotted in Fig. 6(b). The switch between convective heat exchange and dominating viscous heating can be identified by $\mathrm{Nu} = 0$, which corresponds to $x/L \simeq 0.37$, whilst bulk temperature becomes higher than the imposed wall temperature after the vertical asymptote, $x/L \simeq 0.59$.

As widely reported in literature [11, 24–27, 30], the profile of the mean Nusselt number is affected by several parameters:

- Brinkman number and Peclet number, $\mathrm{Pe} = \mathrm{Re}\,\mathrm{Pr}$, defines the flow characteristics;
- aspect ratio and non-dimensional joint radius, which define the geometry of the cross-section .

Knowing the effect of such parameters is crucial in practical engineering problems involving micro-channels heat exchanger optimization [17–20].

Lee et al. [27] proposed a correlation for predicting the mean Nusselt number as a function of axial coordinate in case of negligible viscous heating (i.e. $\mathrm{Br} = 0$),

$$\mathrm{Nu}_c \simeq \frac{1}{C_1\,\tilde{x}^{C_2} + C_3} + C_4 \tag{50}$$

with $\tilde{x}$ the non-dimensional axial coordinate:

$$\tilde{x} = \frac{x}{D_h}\,\mathrm{Pe}^{-1} \tag{51}$$

Regression coefficients C_{1-4} are plotted in [27] as a function of the aspect ratio β defining the rectangular cross section.

Equation (50) is not sufficient for fitting the behaviour of the Nusselt number when the viscous heating source term plays a dominant role in heat transfer process, see Fig. 6(b). Thus, a modified regression model is considered instead,

$$\mathrm{Nu} \simeq \frac{\mathrm{Nu}_v - \mathrm{Nu}_c\,\chi}{1-\chi} \tag{52}$$

$$\chi = \frac{C + \mathrm{Br}}{\mathrm{Br}} \exp\left[-m\,\frac{x}{D_h}\mathrm{Pe}^{-1}\right] \tag{53}$$

where Nu_c can be calculated through Eq. (50).

Applying such a correlation, i.e. Eqs. (52) and (53), for fitting the numerical curve of Fig. 6(b) allows to reach a residual sum of square tolerance of 10^{-2} on 1000 computed values of Nu. Regression coefficient C and exponent m must be determined as a function of the channel cross-section geometry and of the Nusselt number at dominant viscous heating Nu_v. It was verified that the computed values of C and m are not affected by changing Peclet and Brinkman numbers while keeping the cross section geometry fixed, with a discrepancy of $\Delta C/C \sim 1\,\%$, $\Delta m/m \sim 1\,\%$ for $\mathrm{Pe} \in [10^1,\, 10^3]$, $\mathrm{Br} \in [10^{-3},\, 10^{-1}]$. It is worth to point out that coefficients C_{1-4}, C and m are affected by the imposed inlet condition. In accordance to the work of Barletta et al. [23], an adiabatic preparation of the fluid $\Theta_0(\eta,\zeta)$ having bulk temperature $T_i < T_w$ is always considered throughout this paper.

The effect of changing the joint radius on the mean Nusselt number was investigated and the resulting curves are plotted in Figs.7(a) and 7(b), which are referred to fixed Brinkman number and cross section aspect ratio, for both test cases 3T and 4T. It can be noticed that the position x, at which transition between convective to viscous driven heat transfer occurs, decreases with increasing γ, in accordance with the effect of rounding the cross section geometry, which improves heat exchange process. As expected, the effect

γ	C	m	C_1	C_2	C_3	C_4	
0	0.7539	11.83	263.8	1.307	0.1668	3.597	3T
0.25	0.7582	12.26	270.9	1.310	0.1614	3.747	
0.5	0.7674	12.56	276.8	1.311	0.1588	3.859	
1	0.7632	12.60	281.5	1.312	0.1579	3.914	
0	0.9225	12.86	258.0	1.321	0.1674	3.168	4T
0.25	0.9344	13.82	276.1	1.329	0.1575	3.410	
0.5	0.9592	14.57	292.6	1.334	0.1527	3.597	
1	0.9878	15.07	335.9	1.352	0.1506	3.727	

Table 3: Regression coefficients of Eq. (53) for Nusslet number calculation through Eq. (52); $\beta = 3/5$.

of rounding on the computed Nu is stronger for test case 4T, corresonding to 4 rounded corners. The corresponding values of coefficients C_{1-4}, C and m, which allow fitting the numerical results of Figs.7(a) and 7(b) through Eqs. (50), (52) and (53), are reported in Table 3, while the dependence of thermal entrance length, $L_{th}\ :\ \mathrm{Nu}(L_{th}) = 0.95\,\mathrm{Nu}_\infty$, on the Brinkman number and radius is shown in Fig. 8, where the non-dimensional thermal entrance length,

$$\tilde{L}_{th} = \frac{L_{th}}{D_h}\,\mathrm{Pe}^{-1} \tag{54}$$

monotonically decreases for increasing Brinkman numbers in both test cases, 3T and 4T. Note that solution of Eqs. (19) and (26) for a given section geometry allows one to investigate Graetz-Brinkman problem for any value of Pe and Br and for any inlet temperature condition, eigenfunctions $_n$ only depending on duct section geometry and Θ_v being proportional to Brinkman number magnitude.

Thermally developed temperature profiles, corresponding to computed solution at $x > L_{th}$, through the duct cross section are shown in Fig. 9 for Br = 0.1 and $\gamma = 0, 1$. Comparing Figs. 9(a), 9(b) to Figs. 9(c), 9(d) reveals that test case strongly influences the heat transfer process, since higher temperatures are reached when only a portion of the cross section perimeter is heated (test case 3T). On the other hand, the effect of rounding appears to be much more important when the whole perimeter is heated (test case 4T). The dependence of the fully-developed Nusselt number on channel geometry and on both test cases is discussed further later on.

As a further validation, comparing Fig. 9(d) to the numerical results of [33], where the Authors investigated the restrictive case of laminar, fully developed flow with Br $\neq 0$ through a stadium-shaped channel (i.e. $\gamma = 1$) with imposed wall temperature (corresponding to the current 4T test case), reveals the same qualitative temperature profile.

Several simulations were run in order to trace both Poiseuille and Nusselt numbers of the fully (hydrodynamically and thermally) developed flow for different channel geometries, looking for accurate correlations. After a regression analysis, fourth order polynomial correlations were used to fit the fully developed Poiseuille and Nusselt numbers as a function of the non-dimensional joint radius:

$$\mathrm{Po} = \sum_{m=1}^{5} B_m \, \gamma^{m-1} \tag{55}$$

$$\mathrm{Nu}_v = \sum_{m=1}^{5} C_m \, \gamma^{m-1} \tag{56}$$

Coefficients B_{1-5}, C_{1-5} are reported for different channel aspect ratios β in tables 4 and 5. Results for both test cases 3T and 4T are shown. Developed Poiseuille and Nusselt numbers are also plotted as a function of channel cross section geometry in Fig. 10, which clearly shows that the effect of rounding corners is relevant if 4 corners are rounded instead of 2 (i.e. when test case 4T is considered) and the imposed aspect ratio is sufficiently high. The heated perimeter length $\partial\Omega_h$ also plays an important role: comparing Fig. 10(c) to 10(d) reveals that test case 3T may lead to higher Nusselt numbers than T4 at small aspect ratio, while lower Nusselt numbers are obtained applying 3T constraint when $\beta > 1/2$.

8. Conclusion

In this paper the Poiseuille number and Nusselt, both local and average, number of a laminar, thermally developing flow of a Newtonian fluid inside a rectangular microchannel with rounded corners were studied. The effect of viscous heating was taken into account, leading to the so-called Graetz-Brinkman problem, and T boundary conditions were applied along the heated perimeter of the channel cross section.

Numerical simulations were conducted using `MATLAB`® pdetool, a finite-element based solver, in order to compute velocity and temperature fields over the 3D channel domain. After a proper validation with literature data, several configurations involving complex channel section geometries, most of them never considered in the available literature, were investigated through an efficient numerical method in terms of computational costs, looking for new correlations for Poiseuille and Nusselt number prediction. In particular, novel correlations taking into account viscous heating were proposed for: calculation of Nusselt number along channel axial direction in the thermal entrance region, Eqs. (52) and (53); calculation of the developed Poiseuille and Nusselt numbers, Eqs. (55) and (56). Also, the effects of the Brinkman number, heated cross section perimeter and channel geometry (defined by aspect ratio and rounding radius) on heat transfer performances were studied and a connection between thermal entrance length and Brinkman number was found. The results obtained may be useful for microchannel heat sinks design according to Performance Evaluation Criteria [15], since the Poiseuille and average Nusselt numbers are required for evaluation of transferred heat power, friction loss and Entropy Generation Number [16].

As future work, rarefied fluid flows will be studied since rarefaction effects as well as viscous dissipation may be non-negligible at the microscale [8]; a general Robin boundary condition depending on Knudsen number Kn (which is the ratio between molecular mean free path and hydraulic diameter) must be imposed over the perimeter or its heated part, depending on whether the velocity or the temperature fields are investigated. Also the laminar flow of non-Newtonian fluids characterized by power-law viscosity and significant viscous dissipation should be analysed, since they represents a physical problem involved in many engineering applications.

References

[1] M. Ohadi, K. Choo, S. Dessiatoun, and E. Cetegen. *Next Generation Microchannel Heat Exchangers*. Springer, Heidelberg, 2013.

[2] M. Spiga and G.L. Morini. Nusselt numbers in laminar flow for h2 boundary conditions. *Int. J. Heat Mass Tran.*, 39:1165, 1996.

[3] G.L. Morini. Viscous heating in liquid flows in micro-channels. *Int. J. Heat Mass Tran.*, 48:3637, 2005.

[4] M. Geri, M. Lorenzini, and G.L. Morini. Effects of the channel geometry and of the fluid composition on the performances of dc electro-osmotic pumps. *International Journal of Thermal Sciences*, 55:114, 2007.

[5] M. Lorenzini. The influence of viscous dissipation on thermal performance of microchannels with rounded corners. *Le Houille Blanche*, 4:64, 2013.

[6] M. Lorenzini and G. L. Morini. Single-phase laminar forced convection in microchannels with rounded corners. *Heat Transfer Eng.*, 32:1108, 2011.

[7] P. Vocale, G.L. Morini, and M. Spiga. Dilute gas flows through elliptic microchannels under h2 boundary conditions. *Int. J. Heat Mass Tran.*, 71:376, 2014.

[8] P. Vocale, G.L. Morini, M. Spiga, and S. Colin. Shear work contribution to convective heat transfer of dilute gases in slip flow regime. *Eur. J. Mech. B-Fluid*, 64:60, 2017.

[9] C. Aubert and S. Colin. High-order boundary conditions for gaseous flows in rectangular microducts. *Microscale Therm. Eng.*, 5:41, 2001.

[10] S. Colin, P. Lalonde, and R. Caen. Validation of a second-order slip flow model in rectangular microchannels. *Heat Transfer Eng.*, 25:23, 2004.

[11] B. Çetin, A.G. Yazıcıoğlu, and S. Kakaç. Slip-flow heat transfer in microtubes with axial conduction and viscous dissipation − an extended graetz problem. *Int. J. Therm. Sci.*, 48:1673, 2009.

[12] J. Koo and C. Kleinstreuer. Liquid flow in microchannels: Experimental observations and computational analyses of microfluidics effects. *Journal of Micromechanics and Microengineering*, 13(5):568–579, 2003.

[13] A. Sadeghi, M.H. Saidi, and A.A. Mozafari. Heat transfer due to electroosmotic flow of viscoelastic fluids in a slit microchannel. *Int. J. Heat Mass Tran.*, 54(17-18):4069–4077, 2011.

[14] M. Lorenzini, I. Daprà, and G. Scarpi. Heat transfer for a giesekus fluid in a rotating concentric annulus. *Applied Thermal Engineering*, 122:118–125, 2017.

[15] R. L. Webb. *Principles of Enhanced Heat Transfer*. Wiley, New York, 1994.

[16] A. Bejan. *Entropy generation through heat and fluid flow*. Wiley, New York, 1982.

[17] V. Zimparov. Extended performance evaluation criteria for enhanced heat transfer surfaces: heat transfer through ducts with constant wall temperature. *Int. J. Heat Mass Tran.*, 43:3137, 2000.

[18] V. Zimparov. Extended performance evaluation criteria for enhanced heat transfer surfaces: heat transfer through ducts with constant heat flux. *Int. J. Heat Mass Tran.*, 44:169, 2001.

[19] S. Chakraborty and S. Ray. Performance optimization of laminar fully developed flow through square ducts with rounded corners. *Int. J. Therm. Sci.*, 50:2522, 2011.

[20] M. Lorenzini and N. Suzzi. The influence of geometry on the thermal performance of microchannels in laminar flow with viscous dissipation. *Heat Transfer Eng.*, 37:1096, 2016.

[21] S. Ray and D. Misra. Laminar fully developed flow through square and equilateral triangular ducts with rounded corners subjected to h1 and h2 boundary conditions. *Int. J. Therm. Sci.*, 49:1763, 2010.

[22] G.L. Morini, M. Spiga, and P. Tartarini. The rarefaction effect on the friction factor of gas flow in microchannels. *Superlattice. Microst.*, 35:587, 2004.

[23] A. Barletta and E. Magyari. The graetz-brinkman problem in a plane-parallel channel with adiabatic-to-isothermal entrance. *Int. Comm. Heat Mass*, 33:677, 2006.

[24] M.L. Michelsen and J. Villadsen. The graetz problem with axial heat conduction. *Int. J. Heat Mass Tran.*, 17:1391, 1974.

[25] T. Basu and D.N. Roy. Laminar heat transfer in a tube with viscous dissipation. *Int. J. Heat Mass Tran.*, 28:699, 1985.

[26] J.B. Aparecido and R.M. Cotta. Thermally developing laminar flow inside rectangular ducts. *Int. J. Heat. Mass Tran.*, 33:341, 1990.

[27] P.S. Lee and S.V. Garimella. Thermally developing flow and heat transfer in rectangular microchannels of different aspect ratios. *Int. J. Heat Mass Tran.*, 49:3060, 2006.

[28] A. Filali, L. Khezzar, D. Siginer, and Z. Nemouchi. Graetz problem with non-linear viscoelasticfluids in non-circular tubes. *Int. J. Therm. Sci.*, 61:50, 2012.

[29] O. Aydin and M. Avci. Laminar forced convective slip flow in a microduct with a sinusoidally varying heat flux in axial direction. *Int. J. Heat Mass Tran.*, 89:606, 2015.

[30] M. Barışık, A.G. Yazıcıoğlu, B. Çetin, and S. Kakaç. Analytical solution of thermally developing microtube heat transfer including axial conduction, viscous dissipation, and rarefaction effects. *Int. Commun. Heat Mass*, 67:81, 2015.

[31] R. K. Shah and A. L. London. *Laminar Flow Forced Convection in Ducts - A Source Book for Heat Exchanger Analytical Data.* Academic Press, New York, 1978.

[32] J. B. Miles and J. Shih. Reconsideration of nusselt number for laminar fully developed flow in rectangular ducts. an unpublished paper, 1967.

[33] A. Barletta and E. R. di Schio. Analysis of the effect of viscous dissipation for laminar flow in stadium-shaped ducts. *Int. Commun. Heat Mass*, 28:449, 2001.

[34] P. Wibulswas. *Laminar flow heat transfer in non-circular ducts.* PhD thesis, University College London, 1966.

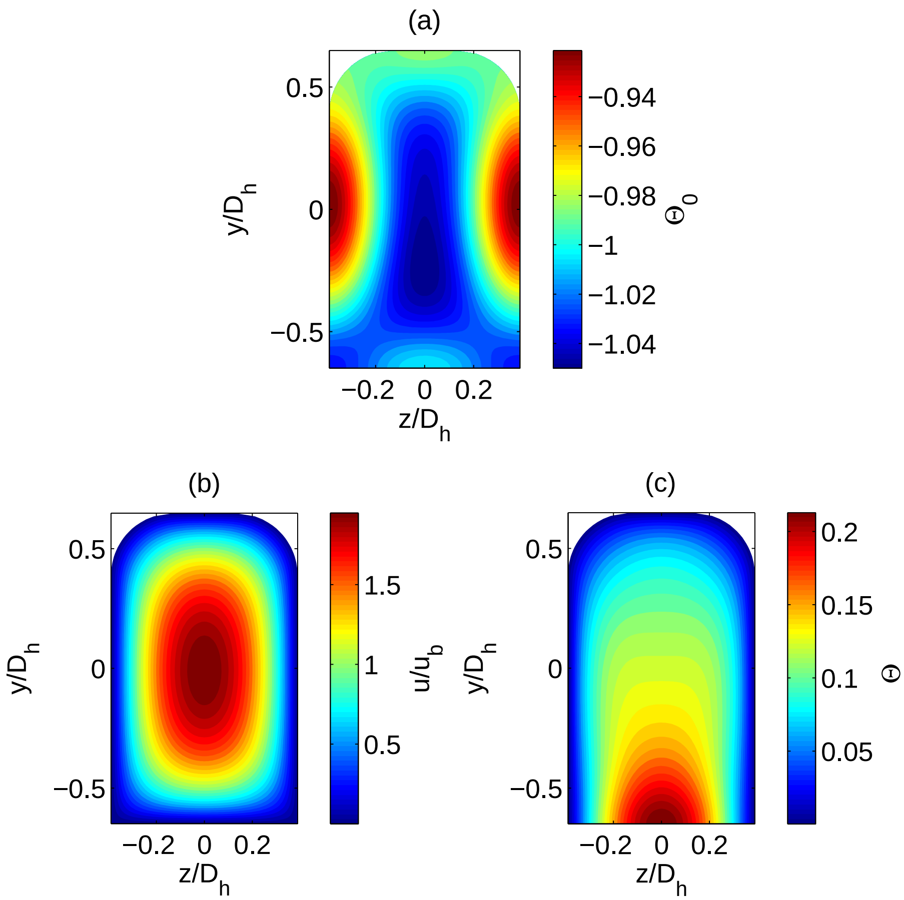

Figure 4: Inlet temperature profile (a), developed velocity profile (b) and developed temperature profile (c). $\mathrm{Br} = 0.1$, $\beta = 3/5$, $\gamma = 2/3$.

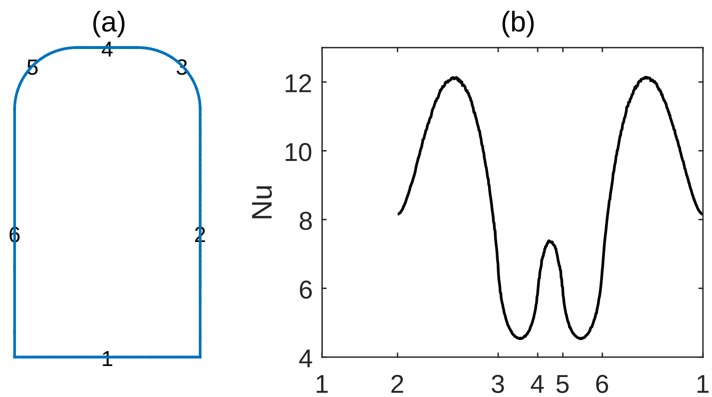

Figure 5: Channel section geometry (a) and local Nusselt number along heated perimeter (b). $\beta = 3/5$, $\gamma = 2/3$.

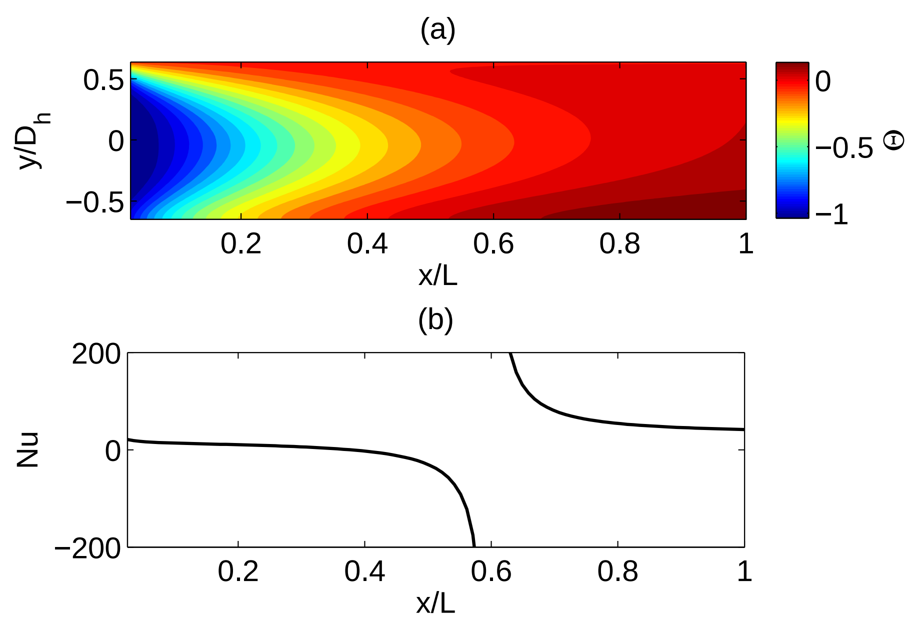

Figure 6: Temperature profile across symmetry section $z = 0$ (a) and mean Nusselt number as a function of axial coordinate (b). Gz $= 3.5$, Br $= 0.1$,
$= 3/5$,γ $= 2/3$.

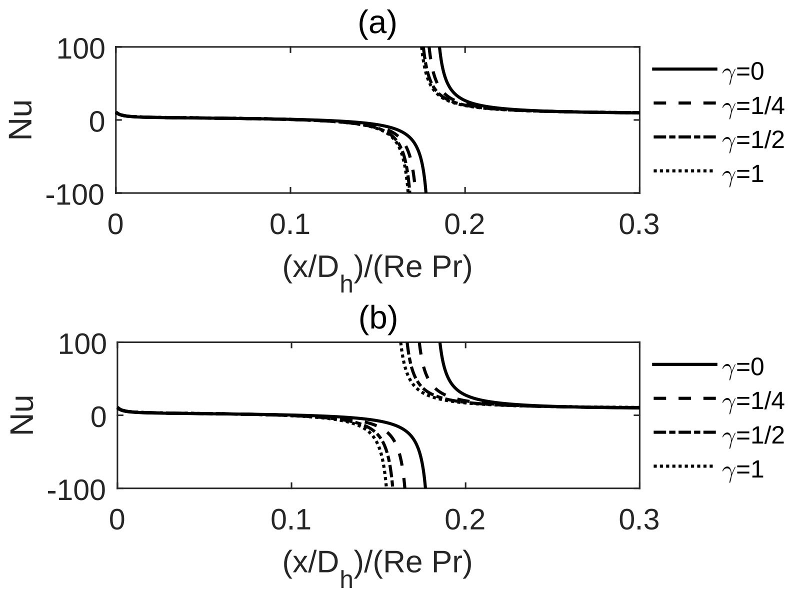

Figure 7: Nusselt number as a function of axial coordinate and non-dimensional joint radius for test cases 3T (a) and 4T (b). $\beta = 3/5$, Br $= 0.1$.

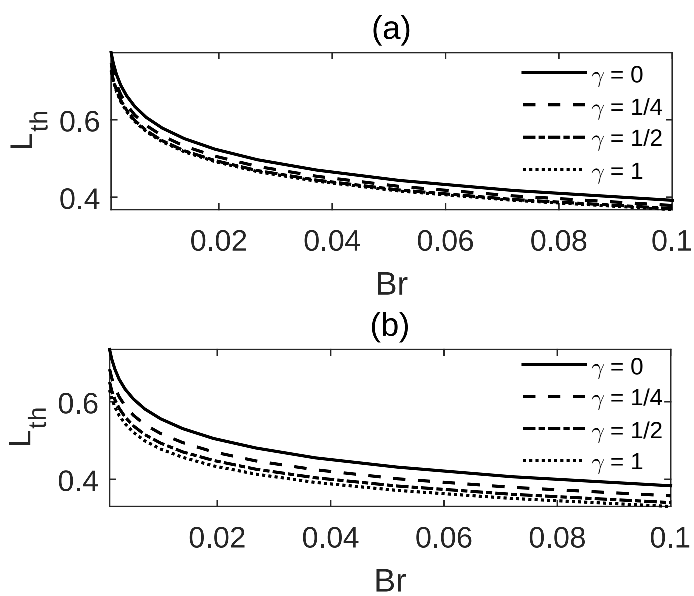

Figure 8: Non-dimensional length of the thermal entrance region as a function of Brinkman number and corner rounding radius: test case 3T (a); test case 4T (b). $\beta = 3/5$.

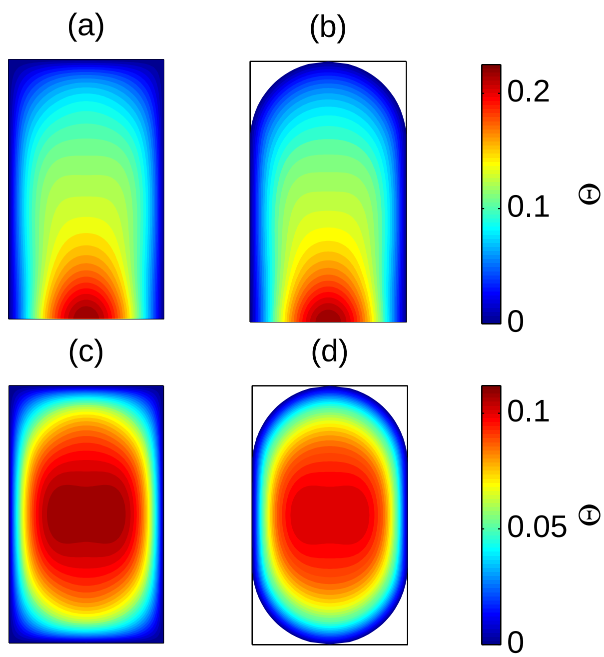

Figure 9: Developed temperature profile for different test cases and cross section geometries: $\gamma = 0$, 3T (a); $\gamma = 1$, 3T (b); $\gamma = 0$, 4T (c); $\gamma = 1$, 4T (d). $\beta = 3/5$, $\mathrm{Br} = 0.1$

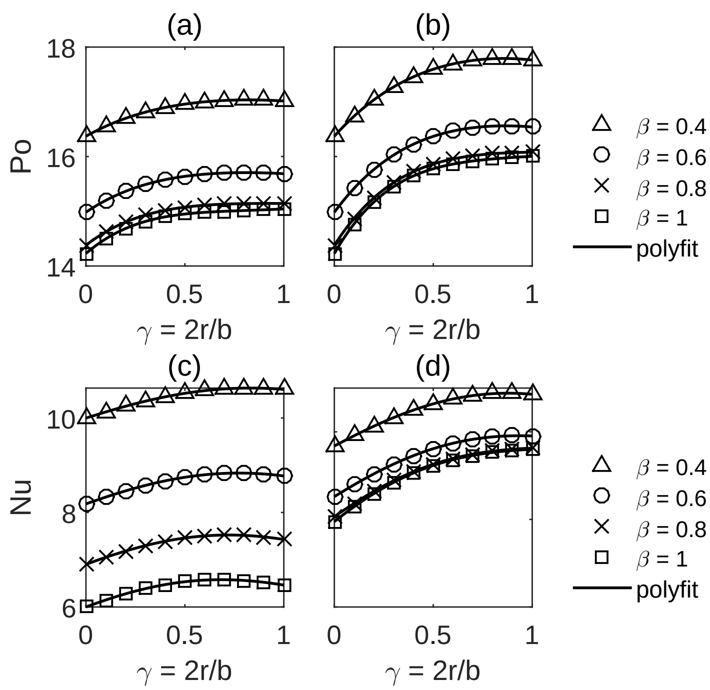

Figure 10: Numerical data vs Eqs. (55) and (56) describing developed Poiseuille and Nusselt numbers as a function of non-dimensional rounding radius and aspect ratio: Po for test case 3T (a); Po for test case 4T (b); Nu_v for test case 3T (c); Nu_v for test case 4T (d).

β	B_1	B_2	B_3	B_4	B_5	
0.05	22.48	0.4619	−0.3860	0.1602	−0.04336	
0.1	21.17	0.8320	−0.7220	0.3068	−0.08366	
0.2	19.07	1.376	−1.281	0.5655	−0.1532	
0.3	17.51	1.753	−1.755	0.8191	−0.2203	3T
0.4	16.37	2.032	−2.186	1.085	−0.2875	
0.5	15.55	2.256	−2.603	1.382	−0.3590	
0.6	14.98	2.451	−3.026	1.718	−0.4393	
0.7	14.61	2.628	−3.455	2.086	−0.5261	
0.8	14.38	2.796	−3.898	2.489	−0.6240	
0.9	14.26	2.959	−4.360	2.930	−0.7383	
1.0	14.23	3.118	−4.837	3.404	−0.8709	
0.05	22.48	0.9239	−0.7573	0.3062	−0.08221	
0.1	21.17	1.664	−1.398	0.5753	−0.1580	
0.2	19.07	2.753	−2.432	1.022	−0.2825	
0.3	17.51	3.509	−3.285	1.439	−0.3939	4T
0.4	16.37	4.068	−4.047	1.866	−0.4950	
0.5	15.55	4.518	−4.781	2.332	−0.5889	
0.6	14.98	4.908	−5.532	2.877	−0.6942	
0.7	14.61	5.264	−6.302	3.481	−0.8095	
0.8	14.38	5.604	−7.122	4.187	−0.9684	
0.9	14.26	5.938	−8.014	5.043	−1.214	
1.0	14.23	6.278	−9.030	6.157	−1.629	

Table 4: Regression coefficients of Eq. (55) for polynomial fit of Po as a function of γ.

β	C_1	C_2	C_3	C_4	C_5	
0.05	16.09	0.3325	-0.07389	-0.1167	0.03890	3T
0.1	14.86	0.5955	-0.1398	-0.2059	0.06557	
0.2	12.82	0.9630	-0.2258	-0.3657	0.1131	
0.3	11.23	1.192	-0.2780	-0.5037	0.1604	
0.4	9.999	1.339	-0.3287	-0.5974	0.1948	
0.5	9.005	1.433	-0.3774	-0.6692	0.2245	
0.6	8.181	1.490	-0.4233	-0.7305	0.2552	
0.7	7.487	1.522	-0.4667	-0.7846	0.2900	
0.8	6.902	1.538	-0.5174	-0.8190	0.3240	
0.9	6.410	1.546	-0.5727	-0.8400	0.3598	
1.0	5.998	1.551	-0.6411	-0.8375	0.3914	
0.05	15.85	0.6514	-0.1568	-0.2019	0.06138	4T
0.1	14.46	1.133	-0.2430	-0.4073	0.1229	
0.2	12.28	1.763	-0.3372	-0.7391	0.2197	
0.3	10.73	2.141	-0.4107	-0.9544	0.2908	
0.4	9.677	2.400	-0.4949	-1.089	0.3644	
0.5	8.977	2.610	-0.6096	-1.160	0.4451	
0.6	8.520	2.803	-0.7648	-1.182	0.5302	
0.7	8.232	2.994	-0.9619	-1.162	0.6126	
0.8	8.061	3.190	-1.211	-1.080	0.6696	
0.9	7.975	3.395	-1.535	-0.8914	0.6611	
1.0	7.949	3.613	-1.955	-0.5454	0.5408	

Table 5: Regression coefficients of Eq. (56) for polynomial fit of Nu_v as a function of γ.